## Werk

**Jahr:** 1985
**Kollektion:** fid.geo
**Signatur:** 8 Z NAT 2148:58
**Digitalisiert:** Niedersächsische Staats- und Universitätsbibliothek Göttingen
**Werk Id:** PPN1015067948_0058
**PURL:** http://resolver.sub.uni-goettingen.de/purl?PPN1015067948_0058

**LOG Id:** LOG_0019
**LOG Titel:** Ray theoretical strong motion synthesis
**LOG Typ:** article

## Übergeordnetes Werk

**Werk Id:** PPN1015067948
**PURL:** http://resolver.sub.uni-goettingen.de/purl?PPN1015067948
**OPAC:** http://opac.sub.uni-goettingen.de/DB=1/PPN?PPN=1015067948



## Contact

Niedersächsische Staats- und Universitätsbibliothek Göttingen
Georg-August-Universität Göttingen
Platz der Göttinger Sieben 1
37073 Göttingen
Germany
Email: gdz@sub.uni-goettingen.de

J Geophys (1985) 58:73–81

Journal of Geophysics

# Ray theoretical strong motion synthesis

**R. Madariaga and P. Bernard**

Laboratoire de Sismologie, Institut de Physique du Globe de Paris, 4 place Jussieu, F.75230 Paris Cedex 05, France

**Abstract.** We present some results of the theory of high-frequency radiation by seismic sources. The emphasis will be placed on the kinematics of high-frequency waves, especially the stopping phases produced when the rupture encounters barriers of general shape. These results will be obtained from the representation theorem in which we replace the Green function by its asymptotic approximation at high frequencies, i.e. what is usually called the far-field approximation. This yields an expression akin to the Kirchhoff diffraction integral used in the modelling of reflection profiles and in seismic migration. The results obtained by this method are valid at distances from the fault which are longer than the dominant wavelength of the radiation. By a detailed analysis of the asymptotic method we find the wavefront discontinuities produced by rupture velocity jumps (barriers) or slip discontinuities (asperities) on the fault. Some examples of comparison between synthetics calculated with the new methods and those obtained by complete near-field synthesis will be presented. Among the examples we will consider is the circular fault, a model proposed by Bouchon for the Coyote Lake earthquake.

**Key words:** Seismology – Elastic waves – Earthquakes

## Seismic radiation

Radiation from a seismic source is a classical problem in elastodynamics. The most recent developments include the study of generalized distributed seismic sources, which we shall review briefly and in an overly simplified fashion.

Let $\mathbf{f}(\mathbf{r}, t)$ be a general distribution of body forces in the earth, where $\mathbf{r}$ and $t$ are position and time, respectively. Seismic radiation may be easily calculated from a representation theorem. The displacement $\mathbf{u}$ is given by:

$$u_i(\mathbf{r}, t) = \int dt \int G_{ij}(\mathbf{r}, t | \mathbf{r}_0, t_0) f_j(\mathbf{r}_0, t_0)\, dV$$

where $V$ is the volume of the earth, $G_{ij}$ is the elastodynamic Green tensor for the earth, which may include both near- and far-field waves. The problem now is to find the body force distribution equivalent to a realistic seismic source. Let $\mathbf{M}(r, t)$ be a seismic moment tensor distribution corresponding to a stress glut, or to inelastic stress in the more traditional nomenclature. The body force distribution equivalent to this moment tensor field is:

$$\mathbf{f} = -\nabla \cdot \mathbf{M},$$

a relation that expresses the equilibrium of forces. Inserting this definition of $\mathbf{f}$ in the representation theorem and integrating by parts, assuming that $\mathbf{M}$ is different from zero only for $t > 0$ and in a finite region, we find:

$$u_i(\mathbf{r}, t) = \int dt \int G_{ij,k}(\mathbf{r}, t | \mathbf{r}_0, t_0)\, M_{jk}(\mathbf{r}_0, t_0)\, dV$$

where the comma indicates differentiation with respect to source coordinates. From the symmetry of $M_{jk}$, we see that the radiation from a point moment tensor source is equivalent to a set of dipoles. A seismic fault may be described as a single layer distribution of moment tensors of the form:

$$M_{jk} = \mu(\Delta u_j n_k + \Delta u_k n_j)\, \delta(D),$$

where $\delta(D)$ is a surface Dirac delta function, $\Delta\mathbf{u}$ is the slip at the fault and $\mathbf{n}$ is the unit normal to it at the point $\mathbf{r}_0$.

Inserting this in the representation theorem, we obtain:

$$u_i(\mathbf{r}, t) = \int \mu\, \Delta u_j * (G_{ij,k} + G_{ik,j})\, n_k\, dS, \tag{1}$$

where the time integration has been replaced by the convolution, indicated by $*$. Using the true Green tensors for the earth is a formidable problem so that we usually take only a part of it, either surface waves or body waves; here we will be concerned only with body waves.

In most studies of earthquake source mechanism it is assumed that, in the vicinity of the fault, the Green function that should be used in Eq. (1) should be calculated exactly including the so-called near-field terms. This leads to very complicated methods for the calculation of accelerograms and seismograms based on plane-wave decomposition and integration by either reflectivity, $f-k$ integration, etc.. It is clear that when broad-band or long-period synthetics are being calcu-

*Offprint requests to:* R. Madariaga

lated, the full Green function is needed in Eq. (1). However, when high-frequency near-source records are desired, it is quite possible to use the so-called far-field Green function in Eq. (1), which basically neglects the coupling between $P$ and $S$ waves. This approximation should be valid as long as the wavelengths under consideration are much shorter than the distance to the fault. In fact, our experience with synthetics indicates that the use of the far-field Green function in Eq. (1) yields reasonable results even at distances of the order of the wavelength! Even for moderately complex structures, the cost of calculating Eq. (1) is reduced by at least an order of magnitude when the asymptotic method is used.

This is not the only advantage of using far-field Green functions in Eq. (1). Since this function may be interpreted in terms of rays, it provides some important insight into the way in which high-frequency waves are generated by very general models of the seismic source. This property will be exploited in order to derive some general results for cracks and dislocation models of the source and to propose a new method for the calculation of near-source synthetics which is quite similar to the Kirchhoff diffraction integral.

In a homogeneous medium the far-field radiation from a point dislocation source may be written in the form:

$$\mathbf{u}(\mathbf{r}, t)=\frac{1}{4\pi\rho c^3}\mathbf{R}^c\frac{1}{D}\delta'(t-R/c) \tag{2}$$

where $\rho$ is density, $c$ is either $P$- or $S$-wave velocity according to the type of wave under consideration. $D$ is the source-receiver distance, $R^c$ is the radiation pattern and $\delta'$ is the derivative of Dirac's delta function. This expression may be generalized to waves obeying simple geometrical optics replacing the term $1/D$ by the geometrical spreading calculated from ray theory. $R^c$ is the radiation pattern which depends on the take-off angle of the ray at the source and its azimuth.

In order to calculate the radiation in the high-frequency approximation we insert Eq. (2) in the representation theorem for a flat seismic fault, Eq. (1). We obtain

$$\mathbf{u}^c(P, t)=\frac{\mu}{4\pi\rho c^3}\int_S \mathbf{R}^c\frac{1}{D}\Delta\dot{u}(t-D/c)\,dS, \tag{3}$$

which is similar to Eq. (14.4) of Aki and Richards (1980) except that we have omitted obvious indices. In Eq. (3), however, $R^c$ and $D$ vary with position on the fault, i.e. we do not make the Fraunhofer approximation. There is some confusion in the literature between far-field or high-frequency approximations like Eq. (2), and the Fraunhofer or far-from-the-source approximation which applies when the observer is at a distance far greater than the dimensions of the source. Our intention is to prove that, within the limits of our theory, accelerograms calculated using Eq. (3) are very good approximations to those calculated with full wave theory including "near-field" terms in Eq. (1).

Equation (3) may be easily generalized to media with slowly varying properties and sharp discontinuities by means of ray theory. However, for the purposes of establishing basic results we shall use the simplified equation, Eq. (3), for a uniform medium. Several of the examples shown later will be calculated for heterogeneous structures using ray theory.

## Source models

Equation (3) is entirely equivalent to the Kirchhoff approximation used in diffraction theory. In the usual interpretation, $\Delta\dot{u}$ represents the field given on a surface. In our application, it represents the slip velocity on the fault. In order to extract further information from Eq. (3) we have to consider realistic models of slip velocity at the source.

The most important feature of $\Delta u$ is that it has a finite support (the ruptured zone) and that this rupture expands with time. We demonstrated in Madariaga (1977) that for very general crack models the radiation of high frequencies will be controlled by the rupture front and that the slip inside the fault will be seen only in the low-frequency approximation. This result may be demonstrated more easily for the so-called dislocation models (it should be more correct to call them dislocation loop models). These models emphasize the rupture front discontinuities and eliminate all the details of the slip function.

We will use a very simple dislocation model for the source: the rupture initiates at the focus $O$ and expands radially with rupture velocity $v$ on the fault plane. In the following discussion, for reasons of simplicity, $v$ will be assumed to be constant; generalization of our results to variable rupture velocity may be obtained in a straightforward way. The slip $\Delta u$ will be assumed to be uniform, constant and parallel to the fault plane inside the rupture front limits. This simple model of the slip function is not physically acceptable but it may be converted into a crack-like dislocation by convolution, as will be discussed later. Let the rupture grow until it reaches a barrier of general shape $L_B$. The slip and the slip velocity are expressed as:

$$\Delta u(r, \theta, t)=D_0 H(t-r/v) H[r_0(\theta)-r] \tag{4}$$

and

$$\Delta\dot{u}(r, \theta, t)=D_0\,\delta(t-r/v) H[r_0(\theta)-r], \tag{5}$$

respectively. Here $t$ is time, $r$ and $\theta$ are polar coordinates on the fault plane, $H$ the Heaviside function, $\delta$ the Dirac function and the equation $r=r_0(\theta)$ is the analytical representation of the barrier line $L_B$. For instance, for a straight barrier line

$$r_0(\theta)=d_0/\cos\theta.$$

The slip velocity (5) is zero everywhere on the fault plane, except on the rupture front where it becomes infinite. This is the model with the maximum possible concentration of slip velocity in the vicinity of the rupture front. In more realistic models the concentration will be spread in a way determined by the stress distribution near the rupture front. For instance, in Haskell's (1964) dislocation model the slip velocity singularity is spread over the rise time $\tau$, so that $\Delta\dot{u}$ will have a boxcar shape. Solutions for these kinds of slip-velocity singularities may be obtained by convolution of our solutions with appropriate source-time functions.

## Crack models

Realistic source models should be based on fracture mechanics, the physics of the processes that occur in the vicinity of the rupture front. Let us assume that the rupture front at the instant $t$ is given by the curve $l(t)$. The main features of the elastic fields near the crack tip may be obtained by assuming steady rupture growth at constant rupture velocity. If we write the elastodynamic equations in polar co-ordinates centred at the rupture front and apply the boundary conditions for cracks, the solution is found to have certain universal features due to the requirement that there be a finite energy flow into the rupture front (Freund, 1979). In this solution the stress and velocity fields present inverse-square-root singularities (see Fig. 1). Along the fault they may be written in the following form:

$$\sigma(x,t)=K[x-l(t)]^{-1/2} \qquad \text{for } x>l(t) \tag{6a}$$

and

$$\Delta\dot{u}(x,t)=V[l(t)-x]^{-1/2} \qquad \text{for } x<l(t). \tag{6b}$$

Here $\sigma$ is a generic stress that represents $\sigma_{xz}$ for antiplane, $\sigma_{zz}$ for in-plane and $\sigma_{zz}$ for tensional cracks, respectively. $K$ is the dynamic stress intensity factor. The definition of $K$ in Eq. (16) differs from the usual definitions in fracture mechanics by a constant ($\sqrt{2\pi}$). We prefer this definition to avoid annoying constants. The slip velocity entering in Eq. (6b) is the appropriate component for each mode of deformation. $V$ is the dynamic velocity intensity factor.

$K$ and $V$ are related by simple expressions:

$$K=\mu/2v\sqrt{1-v^2/\beta^2}\,V$$

for antiplane cracks, where $\mu$ and $\beta$ are the rigidity and shear-wave velocity, respectively, and $v$ is the rupture velocity. For plane cracks,

$$K=\frac{\mu}{2v}\frac{\beta^2 R(v)}{v^2\sqrt{1-v^2/\beta^2}}V,$$

where $R$ is the Rayleigh function:

$$R=4\sqrt{1-v^2/\beta^2}\sqrt{1-v^2/\alpha^2}-(2-v^2/\beta^2)^2.$$

The complete angular dependence of stress and velocity around the crack tip is given by Freund (1979). The inverse-square-root singularities of the form (6) are only valid for rupture velocities lower than the shear-wave velocity for antiplane fractures and the Rayleigh-wave velocity for plane cracks. At these terminal velocities the coefficients of $V$ above reduce to zero, i.e. the dynamic stress concentrations $K$ disappear when the rupture velocity reaches its terminal value.

The stress field is infinite at the rupture front $x=l(t)$. This is the result of the idealization that was made here: it was assumed that the material remained elastic even in the immediate vicinity of the rupture front. The inverse-root singularity appears because this is the only way the elastic field can ensure a finite energy flow into the rupture front. If more realistic conditions are assumed near the rupture front, like a slip-weakening model or a cohesive zone, the singularity disappears. The singularity is associated with the external field, while in the vicinity of the tip we have an internal short-range solution (Rice, 1981; Madariaga, 1983). Both merge smoothly at the border of the cohesive zone. Most of the overall features of crack mechanics may be obtained from the elastic model in which the inelastic behaviour at the breakdown zone is replaced by the global variable $K$. This is valid for the calculation of high-frequency waves if we assume that the size of the breakdown zone is smaller than the wavelength under consideration. Thus, the result we will obtain using ray theory will be valid for a frequency range such that the wavelengths are longer than the breakdown zone and shorter than the distance to the observer.

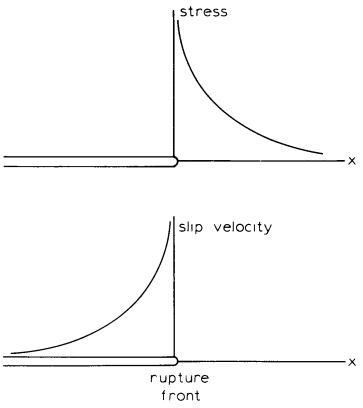


**Fig. 1.** Main properties of the stress and slip velocity fields in the vicinity of a realistic crack model of the rupture front. The rupture is moving to the right with a subsonic rupture velocity

The high-frequency radiation for a crack model may be obtained from that for a dislocation using the slip velocity function as a source-time function, i.e. convolving with Eq. (6a). This method is not exact because it neglects the radiation by stopping phases on the fault (Bernard and Madariaga, 1984a). The results obtained by convolution are, however, reasonably good approximations to the exact ones. Given the uncertainties in the model of the rupture front, we consider the convolved results as largely sufficient for strong motion prediction.

## Kinematics of high-frequency radiation: isochrones

Let us introduce the slip velocity (5) into Eq. (3) to obtain

$$\mathbf{u}^c(P,t)=\frac{\mu D_0}{4\pi\rho c^3}\int_S \mathbf{R}^c\frac{1}{D}\delta[t-\tau(P,\mathbf{r})]\,H[r_0(\theta)-r]\,dS, \tag{7}$$

where

$$\tau(P,\mathbf{r})=r/v+D/c \tag{8}$$

is the retarded time and $dS=r\,dr\,d\theta$. Given a point on the fault $(r,\theta)$, the distance $D$ to the observer at $P$ is

$$D(r,\theta)=(r^2+R^2-2rd\cos\theta)^{1/2}, \tag{9}$$

where $r$, $\theta$, $R$ and $d$ are defined in Fig. 2.

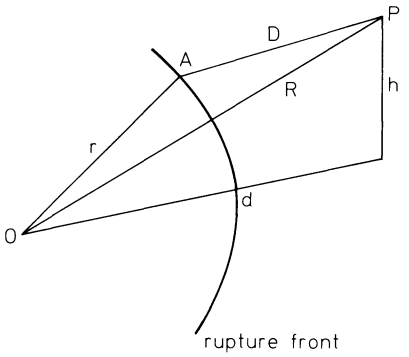


**Fig. 2.** Geometry of the dislocation model. The observer is at $P$, at a height $h$ above the plane of the fault. Point $O$ is the focus, $(r, \theta)$ are polar coordinates: $D$ is the distance from point $A$ to the observer at $P$

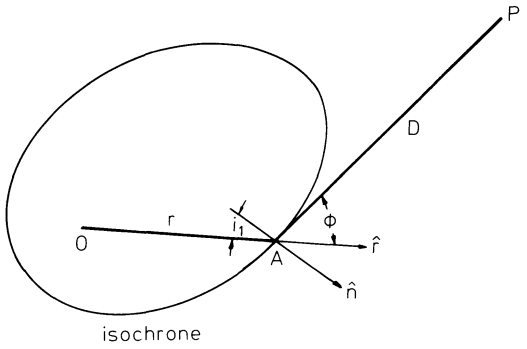


**Fig. 3.** Geometrical properties of the isochrones. Any point $A$ on the isochrone refracts the ray $OA$ in the direction of the observer at $P$. $\mathbf{n}$ is the normal to the isochrone on the fault plane, and $i_1$ is the angle between this normal and the radius from the origin. $\phi$ is the angle of radiation entering into the directivity term

Using the sifting property of the delta function, the surface integral (7) may be reduced to a line integral defined by

$$t=\tau(P,\mathbf{r})=r/v+D(r,\theta)/c. \tag{10}$$

Given the time $t$, Eq. (10) defines a curve on the fault plane that we call the *isochrone*. This curve defines the set of points $[r(t,\theta),\theta]$ on the fault plane from which radiation arrives at the observation point $P$ at time $t$. The different points on the isochrone do not radiate simultaneously but at the time $r/v$ when the rupture front passes through them. We can give a simple geometrical interpretation to Eq. (10): $r/v$ is the travel time of a "rupture ray" that leaves the origin $O$ in direction $\theta$ with velocity $v$ and propagates for a distance $r$ along the fault. At point $A$, of coordinates $(r,\theta)$, it leaves the source and propagates to the observer at $P$ as an elastic wave with velocity $c$.

The equation for the isochrone, Eq. (10), may be easily solved numerically for $r_1=r(t,\theta)$. Let $L_0(P,t)$ be this isochrone which is a function both of the position of $P$ and the time of observation $t$. In a general medium $L_0$ represents a closed curve around the origin. For a homogeneous medium the isochrones $L_0$ are quartic ellipses confocal with the source as shown in Fig. 3.

Changing variables in Eq. (7) from $r$ to $\tau$ we get,

$$\mathbf{u}^c(P,t)=\frac{\mu D_0}{4\pi\rho c^3}\int_0^{2\pi} d\theta \int_{R/c}^{\infty} \mathbf{R}^c \frac{1}{D}\,\delta(t-\tau)\,r(\tau,\theta)\,\partial_\tau r\, d\tau$$

where the partial derivation $\partial_\tau r=\partial r/\partial\tau$ may be calculated from the equation for the isochrone (10):

$$\partial_\tau r=1/(1/v-\cos\phi/c) \tag{11}$$

since $\partial_r D=-\cos\phi$, where $\phi$ is the angle between the radius vector at $r(t,\theta)$ and the direction of the observer (see Fig. 2). Integrating over $\tau$ we get the very simple expression:

$$\mathbf{u}^c(P,t)=\frac{\mu D_0}{4\pi\rho c^3}\int_L \mathbf{R}^c \frac{v}{D(1-v/c\cos\phi)}\frac{dl}{\cos i_1}, \tag{12}$$

where $L$ designates the segments of the isochrone $L_0$ that are inside the fault zone surrounded by the barrier $L_B$; $dl=\cos i_1\ r\,d\theta$ and $(1-v/c\cos\phi)^{-1}$ is the well-known directivity due to the propagation of the rupture front. $i_1$, defined in Fig. 3, is the angle between the isochrone normal and the radius vector from the origin. Thus, Eq. (12) represents the sum of the radiation from a set of point double couples distributed along the isochrone $L$. Each point source is weighted by the local directivity.

Equation (12) provides a very simple method to calculate near-field velocity: at any given time, velocity is given by a simple integral along $L$. We call asymptotic seismograms those calculated using this method. Two approximations were made to obtain Eq. (12), the first one being that the far-field Green function, Eq. (1), be applicable, i.e. that the shortest wavelength $\lambda$ of interest be the less than minimum of $D$. The other approximation, which may be relaxed by convolution, is that $\Delta u$ be strongly concentrated at the rupture front. Let us remark that, since we are summing the radiation from a continuous distribution of sources on the fault, Eq. (12) is not strictly a high-frequency approximation. The true high-frequency approximation to Eq. (12) will be obtained from the analysis of its discontinuities.

Bernard and Madariaga (1984b) obtained Eq. (12) assuming a homogeneous medium and circular rupture propagation at constant velocity. These restrictions were adopted in order to simplify the presentation; in fact Eq. (12) is valid under very general conditions of rupture propagation and for inhomogeneous media as long as ray theory is valid, i.e. for smoothly varying media. We can generalize Eq. (12) to more general models replacing $r/v$ by the time of arrival of the rupture front to a point on the fault and $D/c$ by the travel time from this point to the observer at $P$. In this case, the isochrone is given by

$$t=\tau(P,\mathbf{r})=t_r(\mathbf{r})+T(\mathbf{r},P) \tag{13}$$

where $t_r$ is rupture time at the point $\mathbf{r}$ on the fault, and $T$ is the travel time for a ray from $\mathbf{r}$ to $P$. In Eq. (12), $v$ should be interpreted as the local rupture velocity at point $\mathbf{r}$. Finally, $D^{-1}$ should be replaced by geometrical spreading. Interpreted in this form, Eq. (12) is a very general formula for the calculation of near-field asymptotic synthetics. As shown by Spudich and Frazer

(1984), who independently derived it, it is closely related to the Kirchhoff approximation used in modelling vertical reflection profiles in applied geophysics.

Although Eq. (12) has an extremely simple form, it is difficult to calculate analytically even for a circular dislocation in a homogeneous medium. We proceed in the following way: first, for every given observer we determine a set of equally time-spaced isochrones numerically; this is the most time-consuming part of the computation. Once the isochrones are calculated, we integrate Eq. (12) numerically.

### Example: Coyote Lake earthquake

We shall now apply the asymptotic method to the calculation of synthetic accelerograms for the Gilroy 6 recording of the August 6, 1979 Coyote Lake earthquake in California. This event was studied by Bouchon (1982) who proposed a dislocation model for the source and calculated synthetic accelerograms by a numerical frequency-wavenumber integration method. His model is a vertical strike-slip fault as shown in Fig. 4. Rupture starts at 9.5 km depth and propagates self-similarly with a constant rupture velocity of 2.6 km/s. Slip is constant (dislocation model) and equal to $D_0 = 21$ cm. The final fault shape is defined by a rectangular barrier where rupture stops abruptly. The Gilroy 6 station was practically on the fault trace, 10 km away from epicentre. The medium consists of an upper layer 1.75 km thick, with a shear velocity of 2.4 km/s and a density of 2.6 g/cm$^3$, overlying an elastic half-space with a shear velocity of 3.5 km/s and density 2.8 g/cm$^3$.

The isochrones for regular increments of the observation time are shown in Fig. 4. They were obtained by a numerical solution of Eq. (10) where $D/c$ was replaced by the appropriate expression for the travel time in a layer over a half-space. The separation between neighbouring isochrones is proportional to the directivity factor; the area that radiates the higher amplitudes is the elongated sector pointing from the source to the observation point. This explains why, as will be shown below, the dominating part of the radiation comes from this sector of the fault.

We may now compute synthetic displacement records by integration along the isochrones. Since station Gilroy 6 is practically on the fault plane, only *SH* waves with displacement perpendicular to the fault were considered. The synthetic displacement record obtained by our method is shown in the top of Fig. 5. Theoretically, these asymptotic records are valid for frequencies greater than 1.5 Hz in order that all wavelengths be shorter than the distance to the fault.

In the same figure we present the displacement record computed numerically be Bouchon (1982) for the same model. He discretized the fault into elementary sources and calculated displacement integrating the full near-field radiation for each of these sources. In spite of the different theoretical limits of validity for the two methods, $f < 3.2$ Hz for Bouchon and $f > 1.5$ Hz for the asymptotic method, the two solutions are very similar. The principal high-frequency phases are clearly identified and the general form even at low frequencies is very similar. The asymptotic solutions appear to be valid down to frequencies of 1 Hz in this case. The principal difference between these results is the rapid increase just before phase 2 which does not appear in Bouchon's synthetic. This difference is probably due to the discretization of the source in his model.

As seen in Fig. 4, the isochrones are tangent to the barriers at the points which we call $I_1$ to $I_4$. Radiation from these four points and from the origin is respon-

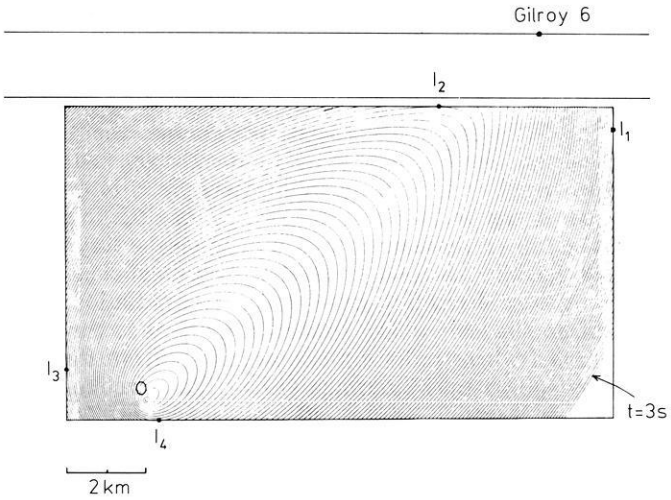


**Fig. 4.** Source model for the Coyote Lake earthquake (after Bouchon, 1982) and the isochrones for station Gilroy 6. The fault plane is vertical and the focus is at depth 9.5 km. The rupture front propagates with constant velocity 2.6 km/s and stops on the rectangular barrier 8 km × 14 km, whose top is at 2 km depth. The station (Gilroy 6) is 10 km from the epicentre, on the fault plane. The slip inside the rupture front is 21 cm (dislocation) in the horizontal direction (strike-slip). The medium has an upper layer 1.75 km thick. The isochrones are plotted for a regular increment of the observation time. They are tangent to the barrier at points $I_1$, $I_2$, $I_3$ and $I_4$

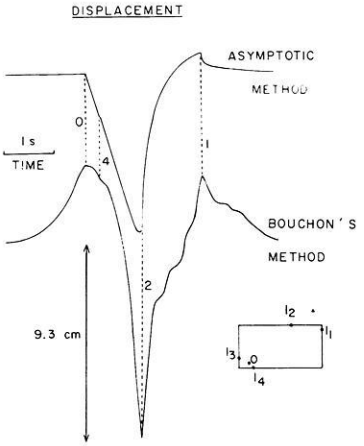


**Fig. 5.** Comparison between the asymptotic method and Bouchon's frequency-wavenumber integration method. The asymptotic displacements calculated by the two methods show a similar overall shape. Phases 0, 1, 2 and 4 in the asymptotic appear clearly in the complete solution, in spite of the different frequency content of either synthetic. The arrival before phase 0 in Bouchon's synthetic is due to near-field low frequencies, which are not modelled in the asymptotic synthetics

sible for the discontinuities of the radiated field. We clearly identify in the synthetics the starting phase (0) and the high-frequency phases generated at the critical points $I_1$ and $I_2$. The radiation from $I_3$ and $I_4$ is weaker because of directivity effects. Just before the arrival time of the phase radiated by $I_2$ the displacement increases rapidly. This is not a barrier effect, but is explained by the very short distance between the interface and the top of the barrier which produces a very rapid decrease with time of the transmission coefficient near $I_2$. It is also interesting to note that the radiation from the corners is very weak. This is in contrast to the Haskell model where radiation comes mainly from the corners as shown by Madariaga (1978). The circular fault model is a much more efficient generator of high frequencies than Haskell's model where strong phases are observed only in front of the fault.

## Radiation from a barrier: critical and stopping phases

The method proposed in the previous sections, based on the Kirchhoff approximation for the Green function, is valid for wavelengths shorter than the distance to the fault. It is, in fact, an intermediate-frequency diffraction approximation to the radiation. At much higher frequencies, those that are of interest in earthquake engineering, we can obtain much simpler approximations to the high-frequency phases or wavefront discontinuities in the signal.

There are two major kinds of discontinuities in Eq. (12), the first ones are the starting phases radiated from the origin of rupture at $O$. These are weak singularities because the isochrone line $L_0$ shrinks to zero as the time $t \to R/c$, the arrival time for the radiation from the origin. Initial phases for the dislocation model (4) behave like $t \cdot H(t)$ in displacement. Since these phases may be easily calculated by standard methods (see Chapter 14 in Aki and Richards, 1980), we will concentrate on the strongest phases which are produced by the interaction of the rupture front and the barrier.

Let us consider the geometry of the barrier and isochrones shown in Fig. 6. Initially, the isochrones $L_0(P, t)$ are continuous curves closed around the origin. As time increases the isochrone eventually becomes tangent to a barrier at a point $I_1$. We call critical time $t_c$ the time that defines this isochrone. In the vicinity of $I_1$, $L_0$ cuts $L_B$ at two points defined by position $s_1$ and $s_2$ along the barrier. As shown in Fig. 6, two geometrical cases have to be considered, depending on the relative curvature at $I_1$ of $L_0$ and $L_B$. We will develop our results for the case of Fig. 6a but, as we show later, the same results apply to the case of Fig. 6b. For times $t < t_c$, the isochrones $L_0$ are continuous, while for $t > t_c$ the isochrone splits, loosing a segment of length $\Delta L$.

Therefore, for times $t > t_c$, the discontinuity of the displacement field $u$ in Eq. (12) may be approximated by:

$$\mathbf{u}^c(P,t) = -\frac{\mu D_0}{4\pi\rho c^3} \int_{\Delta L} \mathbf{R}^c \frac{1}{D} \frac{v}{1 - v/c \cos\phi} \frac{dl}{\cos i_1}, \tag{13}$$

where the minus sign appears because the discontinuity is due to the disappearance of the segment $\Delta L$ from the integral.

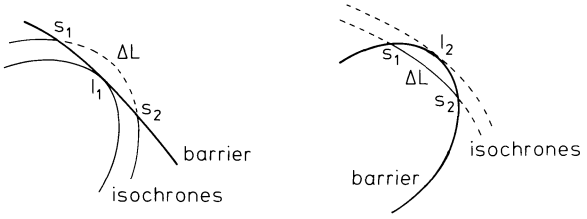


**Fig. 6.** Generation of critical phases by diffraction at a barrier. The isochrone is tangent to the barrier line at $I_1$, or $I_2$ at times $t_c$. In the case of the critical point $I_1$, the isochrone looses a segment of length $\Delta L$ for times greater than $t_c$. At critical point $I_2$, on the other hand, a segment of length $\Delta L$ shrinks to zero as time approaches $t_c$. These two types of singularities generate most of the high-frequency radiation by the source

For $t \simeq t_c$, the segment of integration $\Delta L$ is small and the integral (14) may be approximated by

$$\mathbf{u}^c(P,t) = -\frac{\mu D_0}{4\pi\rho c^3} \mathbf{R}^c \frac{1}{D} \frac{v}{1 - v/c \cos\phi} \frac{\Delta L}{\cos i_1} \tag{18}$$

where $\mathbf{R}^c$, $D$, $\phi$, $i_1$, etc. are calculated at the critical point $I_1$.

In order to evaluate Eq. (18), we have to calculate $\Delta L$ in the vicinity of $I_1$. Let us introduce the travel time $T(s)$ of a ray diffracted in the direction of the observer at a point of coordinate $s$ on the barrier $L_B$:

$$T(s) = r_0(s)/v + D(P,s)/c \tag{19}$$

where $D$ is the distance from the point $s$ on the barrier to the observer at $P$ and $r_0(s)$ is the equation of the barrier. At the point $I_1$ of coordinate $s_c$ the isochrone and the barrier are tangent so that:

$$t_c = T(s_c)$$
and
$$T'(s_c) = \frac{dT(s_c)}{ds} = \frac{d\tau}{dl} \tag{20}$$

where $l$ is distance along the isochrone. Now, since by definition $\tau$ is constant along an isochrone, then

$$d\tau/dl = 0.$$

Thus, the travel time $T(s)$ has an extremum at the point $I_1$ where the isochrone is tangent to the barrier. The arrival time at the observation point $P$ of a critical ray diffracted at point $I_1$ on the barrier is $t_c = T(s_c)$. Also, the angle $i_1$ appearing in Eq. (18) was defined in Eq. (12) as the angle between the rupture front and the isochrone. Since the isochrone is tangent to the barrier at $I_1$, $i_1$ also represents the angle of incidence of the rupture front on the barrier as seen in Fig. 7.

Let us prove now that the extremum condition for the travel time $t_c$ leads to Snell's law for diffraction. By definition of the normal to a plane curve and referring to Fig. 7, we find

$$\frac{dr_0(s)}{ds} = \sin i_1$$

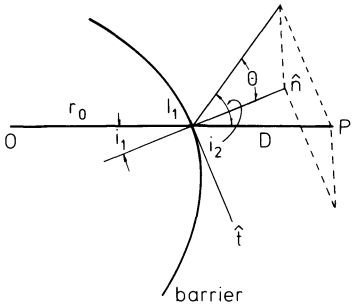


**Fig. 7.** Geometry of diffraction by a barrier of general shape. A "rupture ray" propagating from the source with rupture velocity $v$ is diffracted by the barrier in the direction of the observer at $P$. $i_1$ and $i_2$ are the incidence and diffraction angles, respectively. They satisfy Snell's law for diffraction. $\theta$ is the angle between the fault plane and the plane containing the tangent to the barrier, **t**, and the observation point

and (21)

$$\frac{dD(s)}{ds}=\sin i_2,$$

where $i_1$ is the angle of incidence of the rupture front on the barrier and $i_2$ is the take-off angle of the diffracted wave that passes through $P$. Thus, the second equation in (20) leads to

$$\frac{\sin i_1}{v}=\frac{\sin i_2}{c} \tag{22}$$

which is Snell's law for diffraction.

We may now calculate $\Delta L$ in Eq. (18). Since $T'(s_c)=0$, Taylor's expansion of the travel time $T(s)$ around $I_1$ yields

$$T(s)=t_c+1/2T''(s_c)(s-s_c)^2. \tag{23}$$

Noting that $s_1$ and $s_2$ are located on the same isochrone of time $t=T(s_1)=T(s_2)$, we get from Eq. (23):

$$\Delta L=s_1-s_2=2\frac{\sqrt{2(t-t_c)}}{\sqrt{T''(s_c)}}. \tag{24}$$

For $T''>0$, we have a minimum time phase so that Eq. (24) is valid only for $t>t_c$; this is the situation that prevails in the vicinity of $I_1$. We may now insert Eq. (24) into Eq. (18) to obtain the singularity associated with a critical phase:

$$u^c(P,t)=-\frac{\mu D_0}{2\pi\rho c^3}R^c\frac{v}{1-v/c\cos\phi}\frac{1}{D}\frac{\sqrt{2(t-t_c)}}{\cos i_1\sqrt{T''}}\cdot H(t-t_c). \tag{25}$$

For $T''<0$, $t$ has to be less than $t_c$. This is the case of a maximum time critical phase like the one radiated from $I_2$ in Fig. 6b. In this case we get:

$$\mathbf{u}^c(P,t)=+\frac{\mu D_0}{2\pi\rho c^3}\mathbf{R}^c\frac{v}{1-v/c\cos\phi}\frac{1}{D}\frac{\sqrt{2(t_c-t)}}{\cos i_1\sqrt{-T''}}\cdot H(t_c-t). \tag{26}$$

The different variables appearing in Eqs. (25) and (26) are all evaluated at the diffraction points $I_1$ and $I_2$, respectively. The time dependence of Eq. (26) is the Hilbert transform of that of Eq. (25). The second derivative of the travel time is the usual geometrical spreading for two-dimensional waves. $T''$ is not difficult to calculate for constant rupture velocity and homogeneous medium, but it is much more difficult to calculate in more general situations. For this reason we recast Eqs. (25) and (26) in terms of radii of curvatures of the rupture front $r_1$, the barrier $a$ and the diffracted wavefront $\rho$. Taking the second derivative of Eq. (19), calculated at $s_c$ using Eq. (21), we get:

$$T''(s_c)=\frac{\cos i_1}{v}\frac{di_1}{ds}-\frac{\cos i_2}{c}\frac{di_2}{ds}. \tag{27}$$

The derivatives $di/ds$ may be calculated from simple considerations about the geometry of flat curves. Following Achenbach et al. (1983, pp 175–180), we get:

$$\frac{di_1}{ds}=\frac{\cos i_1}{r_1}-\frac{1}{a}\qquad\frac{di_2}{ds}=-\frac{\cos i_2}{D}-\frac{\cos\theta}{a}, \tag{28}$$

where $\theta$ is the angle between the plane of the barrier and the plane containing the diffracted ray and the local tangent to $L_B$ (see Fig. 7). Inserting in Eq. (27), we find:

$$T''(s_c)=\frac{\cos i_2}{cD}\left[1+\frac{D}{\rho}\right] \tag{29}$$

where $\rho$, the radius of curvature of the critical (stopping) phase, is

$$\frac{1}{\rho}=\frac{c\cos^2 i_1}{v\cos^2 i_2}\frac{1}{r_1}+\left(\cos\theta-\frac{c\cos i_1}{v\cos i_2}\right)\frac{1}{a\cos i_2}. \tag{30}$$

This is the standard relation between the radius of curvature of the diffracted wavefront and the radius of curvature of the incident wavefront $r_1$. In the case of a circular rupture, $r_1=r$.

Finally, reinserting Eq. (29) into Eq. (25) we get

$$\mathbf{u}^c(P,t)=-\frac{\mu D_0}{2\pi\rho c^3}\mathbf{R}^c\frac{v}{1-v/c\cos\phi}\frac{\cos i_2}{\cos i_1}\cdot\frac{\sqrt{2c}}{\sqrt{|1+D/\rho|}\sqrt{D}}S(t), \tag{31}$$

where $S(t)$ is the radiated signal:

$$\sqrt{(t-t_c)}\,H(t-t_c)\quad\text{for } D/\rho+1>0$$
or (32)
$$\sqrt{(t_c-t)}\,H(t_c-t)\quad\text{for } D/\rho+1<0.$$

Equation (31) gives the high-frequency part of the displacement **u**: the critical time $t=t_c$ corresponds to the arrival time of the ray reaching $P$, diffracted at the point $I_1$ on the barrier $L_B$. Thus the critical point $I_1$ seems to radiate the high-frequency signal (stopping phase) that reaches point $P$. For a given barrier $L_B$, the position of the critical point depends on the observer

position $P$ and it may be calculated by two-point ray tracing methods. A "rupture" ray propagates with velocity $v$ along the fault until it reaches the barrier; at that point a cone of diffracted rays that satisfy Snell's law for diffraction, Eq. (22), is generated. One of these diffracted rays passes through $P$. Tracing this ray is a difficult numerical problem since it has to pass through the nucleation point $O$, the diffraction point $I_1$ and the observer $P$. Once ray tracing is done, we can calculate the amplitude using Eq. (31) which may be easily generalized both to inhomogeneous media and to variable rupture velocity using standard dynamic ray tracing (Cerveny and Hron, 1980). The result, Eq. (31), is in the form of geometrical diffraction theory (e.g. Keller, 1962; Achenbach et al, 1983). It corresponds to a generalization of the diffraction of a straight rupture front making an angle $i_1$ with a straight barrier. Equation (31) is very general and contains all results published in the literature for stopping phases produced by dislocation models of arbitrary shape and rupture history, e.g. those of Savage (1966) for an elliptical dislocation, etc.. Let us finally note that for $\rho<0$, Eq. (31) fails at the caustic located at $D=-\rho$ which is a focal point for the diffracted rays (see Bernard and Madariaga, 1984a).

The main use of Eq. (31) is to calculate high-frequency approximations at any distance from the fault. In particular, the dominating part in most synthetic accelerograms generated by dislocation models may be easily calculated with it. As noticed above, Eq. (31) may be generalized to more general models of rupture in heterogeneous media.

A simple example is shown in Figs. 4 and 5, where the arrival of the four principal high-frequency phases is indicated. The discontinuities associated with those arrivals may be easily calculated from Eq. (31), but they are not very easy to verify against Bouchon's (1982) calculation because his method is too low-frequency in displacement. Further tests for velocity and acceleration were presented by Bernard and Madariaga (1984a) in the case of a buried circular fault.

## High-frequency radiation from a crack model

The previous results may be generalized to deal with more realistic seismic source models than a dislocation. Here we will briefly discuss the case in which the slip velocity is that of a crack model, so that it has the characteristic inverse-square-root singularity (6) near the rupture front, i.e. as the rupture front propagates, the slip velocity may be expressed as:

$$\Delta\dot{u}(r,\theta,t)=(t-r/v)^{-1/2}\,H(t-r/v)$$

near the front. Let us consider two particular behaviours of the rupture front when it reaches a barrier.

In the first model we take

$$\Delta\dot{u}(r,\theta,t)=\frac{H(t-r/v)}{\sqrt{t-r/v}}\,H[r_0(\theta)-r], \tag{33}$$

so that slip continues indefinitely once the rupture stops at the barrier line. An alternative model is

$$\Delta\dot{u}(r,\theta,t)=\frac{H(t-r/v)}{\sqrt{t-r/v}}\,H[r_0(\theta)-vt] \tag{34}$$

in which the crack heals simultaneously on the whole radial line of angle $\theta$ when the rupture front reaches the barrier along that line. Between these two extreme models, unfortunately, it seems difficult to construct a realistic model for healing phases without losing the simplicity of the analytical expression (31). A more realistic model for healing will affect the diffraction coefficient $\cos i_2/\cos i_1$ but not the time dependence of the radiation. Given the uncertainties in the models, Eq. (31) is probably sufficient for most applications.

For the first extreme model, the high-frequency displacement is that given in Eq. (31) convolved with Eq. (33). Then Eq. (31) remains valid but $S(t)$ changes to:

$$S(t)\approx(t-t_c)\,H(t-t_c) \quad \text{for} \quad (1+D/\rho)>0$$

and for acceleration:

$$d^2S(t)/dt^2\approx\delta(t-t_c)$$

while, for $(1+D/\rho)<0$, we obtain the Hilbert transformed pulses. For example, the acceleration pulse behaves like:

$$\frac{d^2S(t)}{dt^2}\approx\frac{1}{(t-t_c)}.$$

Thus, the high-frequency acceleration radiated by a propagating crack stopping abruptly is well described by a superposition of $\delta$-like and $1/t$-like impulses, generated at the critical points on the barrier (Bernard and Madariaga, 1984a).

These results are compatible with observed acceleration spectra, for which the high-frequency part is usually flat. If the jump of the rupture velocity is not instantaneous, but takes a time $\Delta t$, the spectral amplitude of acceleration should break down for frequencies greater than $f_{\max}=1/\Delta t$.

## Conclusions

We proposed a new approach to the synthesis of strong ground motion at high frequencies. Two methods were studied. First, an intermediate-frequency asymptotic method similar to the Kirchhoff integral for diffraction, in which the Green function entering in the representation theorem is replaced by its high-frequency approximation (the so-called far-field terms). The method is valid up to wavelengths of the order of the closest distance from the observer to the fault. It can be easily extended by means of ray theory to heterogeneous media and non-uniform rupture propagation.

Analysing the wavefront discontinuities that appear in the Kirchhoff integral, we determine the dominating part of the radiation at high frequencies. These are the critical phases due to the interaction of the rupture front with barriers. In the particular case in which the barrier stops the rupture completely, these are the usual stopping phases. A general expression based on the geometrical theory of diffraction is derived, which can be easily extended by standard two-point ray tracing to inhomogeneous media.

The interest of the method presented here is that once we have solved for the radiation in a uniform medium, we may simply apply ray theory to propagate the

high-frequency signal in a more realistic heterogeneous attenuating medium.

*Acknowledgements.* This work was supported by INAG under contract from ATP Sismogenèse.

IPG contribution N° 837.

## References

Achenbach, J.D., Gautesen, A.K., McMaken, H.: Ray methods for waves in elastic solids. Boston: Pitman Advanced Publishing Program 1983

Aki, K., Richards, P.: Quantitative seismology. San Francisco: Freeman 1980

Bernard, P., Madariaga, R.: High frequency seismic radiation from a buried circular crack. Geophys. J. R. Astron. Soc. **78**, 1–18, 1984a

Bernard, P., Madariaga, R.: A new asymptotic method for the modelling of near-field accelerograms. Bull. Seismol. Soc. Am. **72**, 539–557, 1984b

Bouchon, M.: The rupture mechanism of the Coyote lake earthquake of August 6, 1979 inferred from near field data. Bull. Seismol. Soc. Am. **72**, 745–759, 1982

Červený, V., Hron, F.: The ray series method and dynamic ray tracing in 3-D inhomogeneous media. Bull. Seismol. Soc. Am. **70**, 47–77, 1980

Freund, L.B.: The mechanics of dynamic shear crack propagation. J. Geophys. Res. **84**, 2199–2209, 1979

Haskell, N.H.: Total energy and energy spectral density of elastic wave radiation from propagating faults. Bull. Seismol. Soc. Am. **54**, 1811–1842, 1966

Keller, J.B.: Geometrical theory of diffraction. J. Opt. Soc. Am. **52**, 116–130, 1962

Madariaga, R.: High frequency radiation from crack (stress drop) models of earthquake faulting. Geophys. J.R. Astron. Soc. **51**, 625–651, 1977

Madariaga, R.: The dynamic field of Haskell's rectangular dislocation fault model. Bull. Seismol. Soc. Am. **68**, 869–887, 1978

Madariaga, R.: Earthquake source theory: a review. In: Earthquakes: observation, theory and interpretation, E. Boschi, ed.. Corso 85, Soc. Ital. di Fisica, Bologna, Italy, 1983

Rice, J.R.: The mechanics of earthquake rupture. In: Physics of the Earth's interior, A. Dziewonski and E. Boschi, eds.. Corso 78, Soc. Ital. di Fisica, Bologna, Italy, 1981

Savage, J.C.: Radiation from a realistic model of faulting. Bull. Seismol. Soc. Am. **56**, 577–592, 1966

Spudich, P., Frazer, L.N.: Use of ray theory to calculate high-frequency radiation from earthquake sources having spatially variable rupture velocity and stress drop. Bull. Seismol. Soc. Am. **74**, 2061–2082, 1984

Received February 5, 1985; revised version June 18, 1985
Accepted June 20, 1985